A Methodology for Designing a Lightweight and Energy-Efficient Kinematically Redundant Actuator

Amin Khorasani, *Graduate Student Member, IEEE*, Raphaël Furnémont, Muhammad Usman, Thierry Hubert, Bram Vanderborght, *Senior Member, IEEE*, Dirk Lefeber, *Graduate Student Member, IEEE*, Greet Van de Perre, and Tom Verstraten, *Member, IEEE*

***Abstract*—Redundant actuators enable to distribute power among two motors, which can be selected optimally in terms of efficiency. We propose a methodology that finds effective combinations of motors and gearboxes for a dynamic load, taking into account the constraints, inertia, and efficiency of each component. Focusing on battery-operated robots as an application, it also considers battery pack mass in relation to the energy required by the actuator for multiple hours of operation. Based on this methodology, a prototype of a kinematically redundant actuator for the distal joint of a robot was built. Simulations and experiments are presented to prove the validity of the proposed approach.**

***Index Terms*—Actuator, energy efficient, over-actuated systems, redundant actuators.**

I. Introduction

ENERGY consumption and mass are important considerations for wearable or mobile robots. The electric servo drives commonly used in mobile and wearable robots have high efficiency at the nominal working point. However, their efficiency degrades in low-speed/high-torque and high-speed/low-torque regions of motor operation. A redundant actuator can address this problem. In contrast to single-drive actuators, which consist of only one motor and - if needed - a gearbox, redundant actuators use multiple motors and gearboxes to drive a single output. With multiple motors, each capable of providing high efficiency at different speeds and torques, it becomes possible to divide the output load requirement among multiple motors to have an efficient actuator. As such, it allows to lower energy consumption, as investigated in detail in [1], [2]. However, if the selection of components is not made optimally, the system's overall mass and energy consumption can be excessive. In this study, a lightweight, energy-efficient kinematically redundant actuator with two motors was designed to meet the requirements of a robot arm's distal joint.

Carefully selecting a motor and a transmission is essential to achieve an efficient design. Therefore, several researchers have addressed the matching of an appropriate motor with a suitable transmission considering dynamic load and actuator constraints. Van de Straete et al. [3] introduced a method to discard non-acceptable motors. The gearbox was assumed to have zero inertia and unit efficiency in this work. Additionally, only peak or continuous torque characteristics are considered for motor selection, rather than both at once. In Roos et al. [4], the mechanical efficiency and inertia of the reducers were considered as constants in the selection process. Based on joule losses and the ideal gear reducer, Rezazadeh and Hurst [5] provided analytical expressions for the optimal transmission ratio that maximizes the motor's energetic efficiency. To verify selection feasibility, in [6] a performance index, called the accelerating factor, was defined for commercially available motors. The index was then compared with the loading factor. In order to determine the best performing machine, [7] examined the relationship between accelerating factor and motor dimensions.

Anderson et al. [8] developed a model and optimization-based methodology for selecting a motor and a set of design parameters that minimize reflected inertia, applied to the design of exoskeletons. In Cusimano [9] the proper motor selection for an inertial load was derived from graphical diagrams. Verstraten et al. developed a methodology based on a mechatronic model of the actuator, including a model of the motor's efficiency [10]. They also compared different methods for calculating energy, highlighting the impact of modelling assumptions on the calculated efficiency [11].

Turning trends from a discrete commercial catalog into continuous functions, Meoni and Carricato [12] present a method for selecting an optimal actuator through the fitting of electromechanical parameters which influence motor and reducer operation.

Several studies above discuss the formulations, applications, and benefits of redundant actuation systems for distributing power among motors or energy buffering elements. A well-known example is the Series Parallel Elastic Actuator [13], which is a statically redundant actuator intended to improve actuator consumption. Verstraten et al. [1], [2] proposed a kinematically redundant actuator with two motors and compared

Manuscript received 24 February 2022; accepted 29 June 2022. Date of publication 20 July 2022; date of current version 16 August 2022. This letter was recommended for publication by Associate Editor G. Endo and Editor C. Gosselin upon evaluation of the reviewers' comments. This work was supported by Research Foundation Flanders (FWO) SBO project ELYSA Project under Grants S001821N, 12Z7920N, and 1505820N. *(Corresponding author: Amin Khorasani.)*

Amin Khorasani, Raphaël Furnémont, Muhammad Usman, Thierry Hubert, Dirk Lefeber, and Tom Verstraten are with the Brubotics, Vrije Universiteit Brusse, and Flanders Make, Brussels, Belgium (e-mail: amin.khorasani@vub.be; raphael.furnemont@vub.be; musmans@live.com; thierry.rene.hubert@vub.be; amin.khorasani@vub.be; tom.verstraten@vub.ac.be).

Bram Vanderborght and Greet Van de Perre are with the Brubotics, Vrije Universiteit Brussel, and IMEC, Brussels, Belgium (e-mail: bram.vanderborght@vub.ac.be; greet.van.de.perre@vub.be).

Digital Object Identifier 10.1109/LRA.2022.3192637

This work is licensed under a Creative Commons Attribution 4.0 License. For more information, see https://creativecommons.org/licenses/by/4.0/

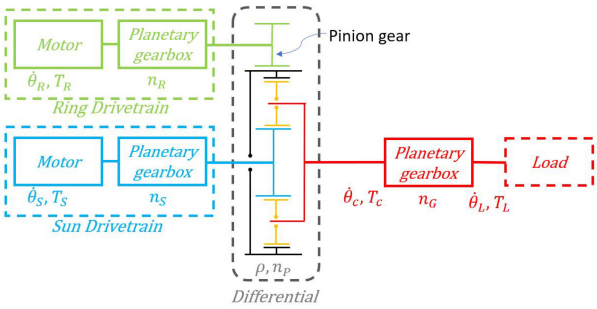

Fig. 1. Schematic of dual motor actuator.

it to an equivalent single-drive actuator in terms of operating range, maximum acceleration, and energy consumption. Girard and Asada investigated a similar redundant actuator for linear motion applications [14]. Babin et al. discussed different uses of a planetary gear system for achieving dual-motor actuation [15].

Choosing appropriate components for a redundant actuator and distributing the power among multiple motors is complicated, since both aspects are intrinsically linked to each other and to the task at hand. A procedure for designing an energy-efficient and lightweight redundant actuator for a specific use case is unfortunately still lacking. Therefore, in this work, we present a methodology for selecting components of a redundant actuator, taking into account the dynamics of the actuator and various losses. We focus on the minimization of energy consumption, while evaluating the mass of the proposed solutions.

The paper is organized as follows. Section II introduces the structure of the actuator, its model, and the applicable constraints. Section III describes the optimization problem and the search algorithm, and introduces the proposed design scenarios. Section IV presents the simulation results of the proposed scenarios and discusses the effect of battery pack mass on actuator selection. The experimental setup is described in Section V. Finally, Section VI concludes the paper.

II. Kinematics and Dynamics Model

A. Actuator Structure

Fig. 1 illustrates a schematic of the Dual-Motor Actuator (DMA). The sun drive-train consists of a motor and a gearbox connected to the sun gear of a planetary gearset (blue components). The ring drive-train consists of a motor and a gearbox coupled to a pinion (Green components). This pinion is engaged by a gear attached to the ring gear of the planetary gearset (black component). The differential consists of a planetary gear set, and a pair of gears attached to the ring gear. An additional gearbox is connected to the carrier (red component). The DMA is a kinematically redundant actuator with two motors, which means that the output rotation is a kinematic superposition of each motor rotation. Hence, the speed distribution between the two motors can be chosen while the torque applied by each motor is imposed by the task. Verstraten et al. studied the kinematics and dynamics of this actuator extensively in [1].

B. Actuator Kinematics and Dynamic Model

The equations for the DMA are presented below. The full derivation of these equations can be found in [1].

In a kinematically redundant actuator, the output speed is a (weighted) sum of each input speed. It is expressed in the following way for the DMA in relationship to its design parameters:

$$\dot{\theta}_L = \frac{1}{n_G}\left(\frac{1}{n_S(1+\rho)}\dot{\theta}_S + \frac{\rho}{n_R n_P(1+\rho)}\dot{\theta}_R\right) \tag{1}$$

where $\dot{\theta}_L$ is the load (output) speed and $\dot{\theta}_S$ and $\dot{\theta}_R$ are the sun and ring drive-train motor (input) speeds, respectively. ρ is the ring-to-sun gear ratio, n_G is the output gearbox ratio, and n_P is the ratio of the gear attached to the ring of the differential. Finally, n_R and n_S represent the ring and sun gearbox ratios as depicted in Fig. 1.

The actuator's dynamics formulation can be described as follows:

$$T_{2m} = [A\dot{x} + BT_c] \tag{2}$$

with

$$T_c = \eta_G^{-\text{sign}(T_L\dot{\theta}_L)}\frac{1}{n_G}T_L + n_G\ddot{\theta}_L J_G \tag{3}$$

Here, we defined $T_{2m} = (T_S, T_R)^T$, with T_S and T_R the torques of sun and ring motor, respectively. T_c is the carrier output torque, T_L is the load torque, η_G is the output gearbox efficiency, and J_G represents its inertia. x is state space form given by

$$x = \begin{bmatrix}\dot{\theta}_S \\ \dot{\theta}_R\end{bmatrix} \tag{4}$$

The Jacobian matrix J is defined as:

$$J = \begin{bmatrix}\frac{1}{n_S}\frac{1}{1+\rho} & \frac{1}{n_R n_P}\frac{\rho}{1+\rho}\end{bmatrix} \tag{5}$$

and

$$A = \begin{bmatrix}J_S & 0 \\ 0 & J_R\end{bmatrix} + J_C BJ$$

$$B = \begin{bmatrix}\frac{C_S}{n_S}\left(\rho C_{PG}+1\right)^{-1} \\ \frac{C_R}{n_R n_P}\left(\frac{1}{\rho C_{PG}}+1\right)^{-1}\end{bmatrix}$$

In the formulas above, J_S and J_R represent the inertia of the sun and ring motor, respectively, and the inertia of the carrier is denoted by J_C. C_R and C_S represent the efficiency function of the gearboxes at sun and ring drive-train. C_{PG} is the planetary differential efficiency function which is calculated with the following formula:

$$C_{PG} = \eta_{PG}^{\text{sign}\left[T_c\left(\frac{\dot{\theta}_S}{n_S(\rho+1)}-\dot{\theta}_c\right)\right]} \tag{6}$$

In the formula above, η_{PG} is differential efficiency, and $\dot{\theta}_c$ is the output speed of the carrier. The motor's coulomb and viscous friction coefficients are important factors, but they are often not included in the motor catalogs directly. These factors were not considered in this study. Furthermore, gearbox efficiency has been assumed to be constant, while in reality the efficiency is speed and torque dependent [16]. Typically, these data types do not appear on the data sheets for gearboxes, and it is not easy

to measure these values for all possible combinations of motors and gearboxes.

C. Constraints

Three categories of constraints have been incorporated into the design scenario, namely pre-processing, processing, and post-processing. When a combination (consist of motors and gearboxes) is selected, its pre-processing constraints ensure it can handle the output requirements' peak speed and peak torque. These constraints are:

$$\left(\frac{1}{n_S}\dot{\theta}_{S,\max} + \frac{\rho}{n_R n_P}\dot{\theta}_{R,\max}\right) > \max\left(n_G(1+\rho)\left|\dot{\theta}_L\right|\right) \quad (7)$$

$$\min\left(n_S C_S T_{S,\max} \;,\; n_R n_P C_R \frac{1}{\rho} T_{R,\max}\right) > \max\left(\frac{1}{n_G(1+\rho)C_{PG}}\left|T_L\right|\right) \quad (8)$$

In the above constraints, $\dot{\theta}_{S,\max}$ and $\dot{\theta}_{R,\max}$ are the maximum permissible speeds of the sun and ring drive-train motors, respectively. Equation 7 derived of kinematics of the actuator presented in (1). Also, $T_{S,\max}$ and $T_{R,\max}$ represent the maximum torques on the sun and ring drive-train motors, which are limited to $\sqrt{2}$ times their nominal values. In the above equations, $\min$ and $\max$ before brackets are minimum and maximum functions, respectively.

During the optimal power distribution between two motors along the output trajectory, the processing constraints must be applied at every stage of the simulation. Initially, combinations are restricted by their motor speed. As a result, each motor is limited to its maximum speed range under the following conditions:

$$\begin{aligned}\left|\dot{\theta}_S\right| &< \dot{\theta}_{S,\max} \\ \left|\dot{\theta}_R\right| &< \dot{\theta}_{R,\max}\end{aligned} \quad (9)$$

Electric motors are subject to two current limits, continuous and peak current. If the robotic application does not operate at a constant torque/ current, we can substitute the RMS (root mean square) value for the value of continuous torque/current. The maximum intermittent (peak) current is another limitation of the current. This is the maximum current that can be achieved within a short period of time. It is not mentioned in the motor's data sheet and depending on the thermal time constant winding can be higher than the nominal values in an instant. For a safe region, it is considered to be $\sqrt{2}$ times of nominal values in this research.

$$\begin{aligned}|T_S| &< T_{S,\max} \\ |T_R| &< T_{R,\max}\end{aligned} \quad (10)$$

The same constraint applies to the gearboxes. It is possible to expect a peak torque greater than a gearbox maximum continuous output torque for a short period of time. We consider the intermittent torque capability of each gearbox for a short time as a constraint during the trajectory simulation. Additionally, the voltage applied to the motor should not exceed the power supply voltage.

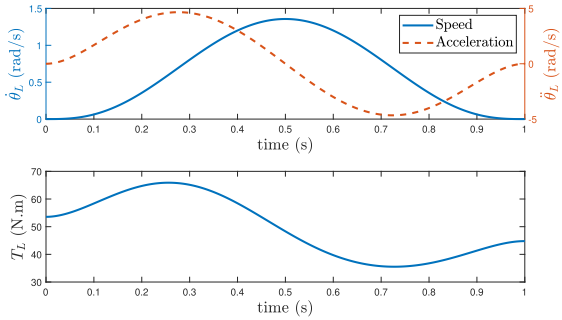

Fig. 2. The torque, speed and acceleration profile representing the actuator requirements.

$$\begin{aligned}k_{tS}\dot{\theta}_S + R_S I_S &< U_{max} \\ k_{tR}\dot{\theta}_R + R_R I_R &< U_{max}\end{aligned} \quad (11)$$

In above constraints, U_{max} is the maximum power supply voltage, which in our case is 60 V, k_{tS} and k_{tR} are the torque constant values for the sun and ring motor, and R and I are the terminal resistance and current of each motor.

The post-processing constraints ensure that the motors and gearboxes can operate continuously. Thus, the RMS value of each motor's torque should not exceed the continuous rated torque of each motor. Similarly, the RMS output torque of each gearbox must be lower than the continuous operation torque listed in the catalog. If λ corresponds to the output torque of the sun motor (S), ring motor (R), or gearboxes, and cont refers to the continuous torque of each component then:

$$\text{RMS}\left(T_\lambda\right) < T_{\lambda,\text{cont}} \quad (12)$$

III. Methodology and Optimization Procedure

A. Optimization and Selection Procedures

A particular torque and speed trajectory, depicted in Fig. 2, will be imposed upon the actuator. Even though a trajectory that stimulates all possible operating points of an actuator is more appropriate for actuator selection, it will make the methodology more complicated and time-consuming, so a simple trajectory consisting of peak requirement values and almost the same values for continuous operation can be chosen instead.

The selection of an actuator combination is done according to the flow diagram depicted in Fig. 3.

After defining the output requirements, a combination of motors and gearboxes is selected from list in nested 'For' loops. After that, pre-processing constraints as described in inequalities 7, 8 are applied.

Then, the optimal power distribution should be determined between the two drivetrains. Therefore, it is necessary to know the speed and acceleration of each motor to solve dynamic (2). Output trajectory is given in Fig. 2, while input trajectories can be determined freely, so actuator equations cannot be determined. To solve this, for one motor (for example, the sun motor), a range of speeds was given to determine speed and acceleration of other motor. The other motor's speed was calculated using

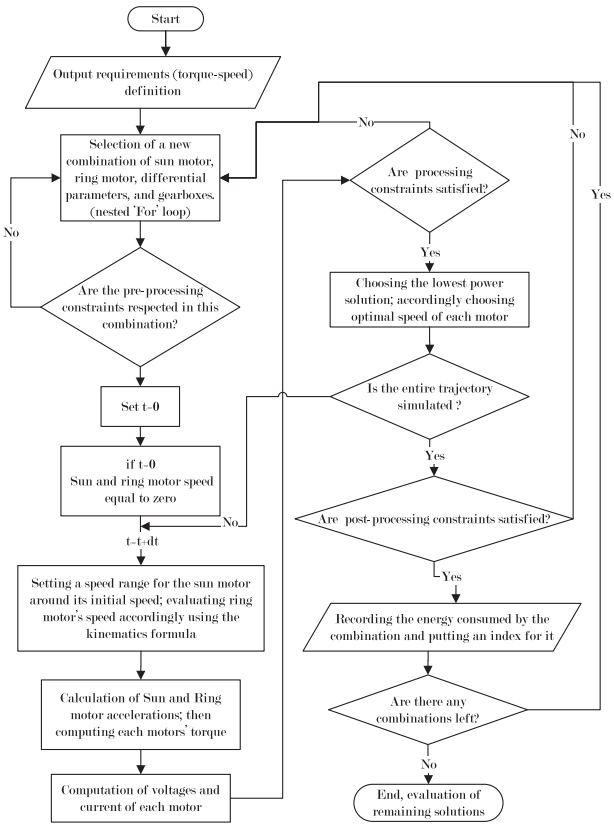

Fig. 3. Flow diagram of methodology approach for DMA component selection.

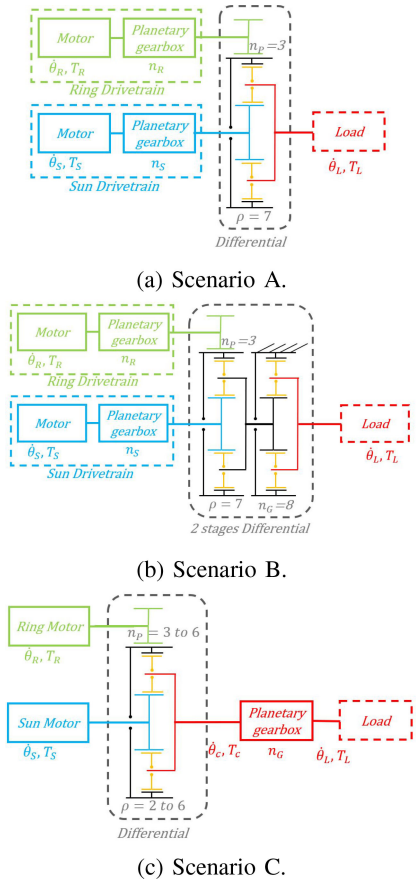

(a) Scenario A.

(b) Scenario B.

(c) Scenario C.

Fig. 4. Different design scenarios for selecting of DMA components.

kinematic (1). The speed range for every step at one millisecond ($dt = 1$ ms) is selected between $[-100; 100]$ revolutions per minute with an interval of 0.5 revolutions per minute around the previous step. A linear approximation was used to calculate the acceleration of each motor. Simulation of output trajectory is performed once every millisecond. Thus, this linear approximation on acceleration, although not exact, can provide a reasonable approximation at a short interval time. As a result of determining the dynamic equation, the voltage and current of each motor can be determined.

Processing constraints including the voltage, speed, and current restrictions expressed by equations (10) and (11). Afterward, the actuator's electrical power is determined. If there are multiple solutions, the solution with the smallest electrical power is recorded. If there is no solution, another combination of motors and gearboxes will be selected, and the process will start over. The process is repeated until the entire trajectory has been evaluated.

Finally, if the selected combination is capable of meeting the task, post processing constraints are applied. If these are met, the combination is recorded for further evaluation. This process is repeated until all combinations have been considered. Finally, from all possible combinations that could perform the task, the combinations with the lowest energy consumption within different mass categories are chosen.

A selection of over 80 Maxon brushless motors of varying power ratings is considered in the analysis. These include motors from the EC, EC-max, EC-flat, ECi, EC-4pole, and IDX series. In addition, we selected gearboxes of the same brand to match the chosen motor on the ring and sun drive-trains. The planetary gear set or pair of gears attached to the differential can also be selected in a variety of types and ratios. In total, over one million combinations are possible with these motors and gearboxes. Instead of simulating all possible combinations, we are simulating a few specific scenarios.

B. Design Scenarios

Different implementations of the DMA are depicted in Fig. 4.

- Scenario A: No output gearbox; single-stage differential with fixed design parameters (Fig. 4(a)).
- Scenario B: Two-stage differential with fixed parameters in a unit cage (Fig. 4(b)).
- Scenario C: No gearboxes in the sun and ring drive-train; high-ratio commercial gearbox at the output. Differential parameters vary to allow for more motors to be used in the sun and ring drive-trains (Fig. 4(c)).

In the calculations for kinematics and dynamics, we set the ratio and efficiency to one and the inertia to zero to account for the components that have been removed in the above scenarios.

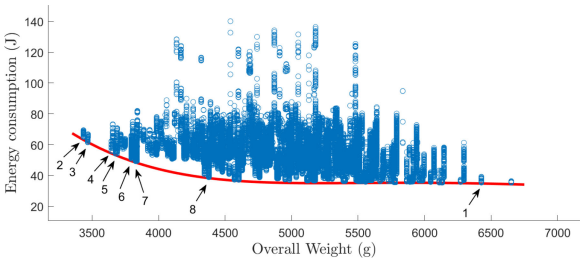

Fig. 5. Energy consumption of possible DMA designs for scenario A. The Pareto frontier is indicated in red line.

IV. Simulations and Discussion

A. Scenario A

As illustrated in Fig. 4(a), the differential output is connected directly to the load, which eliminates the output gearbox mentioned in Fig. 1. For the differential, we have chosen a fixed high-ratio planetary gear ratio ρ=7. Selecting a high-ratio differential, as explained in [2], minimizes the number of stages of the sun and ring gearboxes, avoiding the efficiency penalty associated with extra gearbox stages. For the ring drive-train, we selected a pair of spur gears with a fixed ratio of $n_P = 3$. There is no single-stage gearbox option in the Maxon catalog which meets our high torque requirements for the differential. We therefore instead selected gearboxes from the Neugart PLE080 series, which have a mass of 2 kilograms and an efficiency of 92 percent. A metal version with a width of 10 millimetres was designed for the spur gear attached to the differential. Mass of this gear set is approximately 100 grams. Thus, a fixed mass of 2.1 kilograms is added to the variable mass of the motors and gearboxes in the sun and ring drive-train. By performing the search algorithm described in the Section III on the available combinations, the result of the remaining solutions depicted in the Fig. 5.

Results show that selecting a combination of motors and gearboxes that is energy-efficient is clearly superior to selecting random combinations. The results also indicate that there is a trade-off between choosing a lightweight actuator or an energy-efficient one. Fig. 5 illustrates the trend of energy-optimized solutions using the Pareto frontier curve, as explained in [17]. The Pareto frontier curve is an 8-order polynomial trajectory fitted with the optimal data in different weight categories using least squares method. Those combinations that contradict the trend are manually excluded. The Pareto frontier presented in Fig. 5 shows a tendency toward a lower energy consumption when choosing larger and heavier motor combinations, with a plateau of energy consumption at around 4.5 kilograms and beyond.

In Table I, it can be seen that the first row is the most energy efficient option. This actuator weighs approximately 6.4 kilograms. The best solution in terms of mass (bottom left corner of Fig. 5) weighs 3.4 kilograms, but requires 64.8 joules of energy to complete the task, which is 82 percent higher than the most energy-efficient solution. It is evident from Fig. 5) that combinations far from the Pareto frontier can add a substantial amount of mass and energy to the system.

TABLE I
Motor and Gearbox Combinations for the DMA of Scenario A, Selected From the Pareto Frontier. The First Design is the Most Energy-Efficient, the Second Design Has the Lowest Mass

rows	Sun branch motor	Sun branch PG	Ring branch motor	Ring branch PG	Energy (J) (extra percent)	Mass (g) (extra percent)
1	IDX 56 L, 400 Watt,48v	GPX52-1:44	IDX 56 L, 400 Watt,48v	GPX52-1:103	35.3 (0)	6427 (0)
2	EC-4pole, 200 Watt, 48 v	GP42c-1:113	EC 45 flat, 80 watt,24v	GP42c-1:66	64.8 (82)	3435 (-46)
3	EC-4pole, 200 Watt, 36 v	GP42c-1:113	EC 45 flat, 90 watt,60v	GP42c-1:81	61.4 (74)	3467 (-46)
4	EC 60 flat,150 Watt,36 v	GP52c-1:26	EC 45 flat, 90 watt,36v	GP42c-1:91	55.9 (58)	3645 (-43)
5	EC 60 flat,150 Watt,36 v	GP52c-1:26	EC 45 flat, 80 watt,48v	GP42c-1:81	54.1 (53)	3677 (-43)
6	EC 45 flat, 90 watt,48v	GP42c-1:126	EC 60 flat,150 Watt,48 v	GP52c-1:74	50.91 (44)	3795 (-41)
7	EC 45 flat, 120 watt,60v	GP42c-1:126	EC 60 flat,150 Watt,48 v	GP52c-1:74	49.22 (39)	3827 (-40)
8	IDX 56 L, 350 Watt,48v	GPX52-1:28	EC 45 flat, 80 watt,48v	GP42c-1:126	38.81 (10)	4377 (-32)

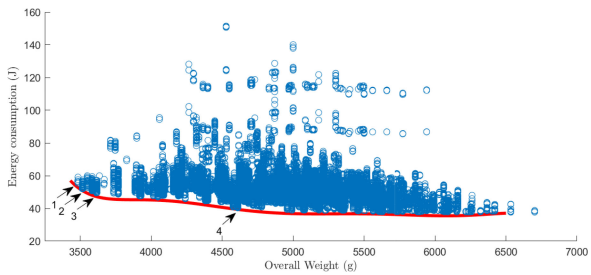

Fig. 6. Combinations with a different mass and energy consumption in the case of using a two-stage DMA.

TABLE II
Motor and Gearbox Combinations for the DMA of Scenario B, Selected Combinations in Fig. 6

rows	Sun branch motor	Sun branch PG	Ring branch motor	Ring branch PG	Energy (J)	Mass (g)
1	EC 45 flat,120 Watt,24v	GP52c-1:12	EC 45 flat, 90 watt,48v	GP42c-1:26	55.4	3484
2	EC 45 flat, 80 watt,60v	GP42c-1:6	EC 45 flat, 80 watt,60v	GP42c-1:26	52	3514
3	EC 45 flat, 80 watt,24v	GP42c-1:15	EC 45 flat, 80 watt,24v	GP42c-1:26	49.5	3614
4	EC 45 flat, 90 watt,48v	GP42c-1:19	IDX 56 M, 350 W, 48v	GPX52-1:6.6	40.8	4577

B. Scenario B

The sun and ring drive-trains described in the scenario A require a high ratio gearbox, usually consisting of at least three stages. These gearboxes have a low efficiency. To increase their efficiency, the main priority is to reduce the number of stages. To achieve this objective, we propose to replace the single-stage differential with a two-stage differential (Fig. 4(b)). With this design, the torques applied to the ring and sun would be lower than in the previous scenario, and the motor and gearbox losses can thus be expected to be lower as well. Although the second stage of the differential reduces the overall efficiency, it may reduce the overall mass of the actuator.

To simplify the search and optimization algorithm, the parameters of the differential have been fixed. As an estimation of the mass of the differential, it is considered to be a 2 stage Neugart PLE080 series, which has a mass of 2.5 kilograms, and considering the suggested spur gears for attaching the ring drive-train to differential, the overall fix mass could be 2.6 kilograms. The overall mass of the lightest combinations in Fig. 6 is little higher than the lightest combinations of scenario A. Moreover, these solutions require less energy. Table II also indicates that, as expected, the ratios of the sun and ring branch gearboxes have been reduced.

Similar to the previous design scenario, heavy combinations tend to be more energy-efficient, whereas lightweight solutions

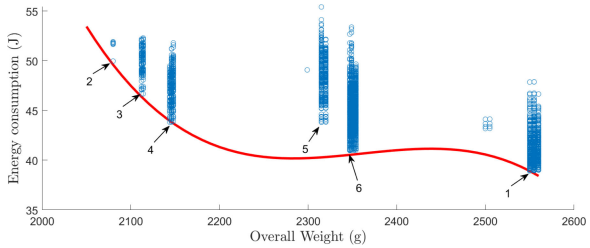

Fig. 7. The energy consumption of different combinations in scenario C. Different ratios are used for differential and spur gears on the ring gear. To this combination, we added 1.5 kilograms for the Apex gearbox and 0.35 kilograms for the differential and spur gears.

TABLE III
MOTOR AND GEARBOX COMBINATIONS FOR THE DMA OF SCENARIO C, SELECTED FROM THE PARETO FRONTIER

Index	Sun branch motor	Ring branch motor	ρ	n_P	n_G	Energy requirement (J) (extra percent)	Mass (g) (extra percent)
1	EC 60 flat, 150 Watt, 48 v	EC 60 flat, 150 Watt, 48 v	3	5	80	38.92 (0)	2550 (0)
2	EC 45 flat, 90 watt, 48 v	EC 45 flat, 90 watt, 48 v	6	6	80	49.96 (26)	2080 (-18)
3	EC 45 flat, 80 watt, 60 v	EC 45 flat, 90 watt, 48 v	6	6	80	46.67 (17)	2112 (-17)
4	EC 45 flat, 80 watt, 60 v	EC 45 flat, 80 watt, 24 v	6	6	80	43.82 (10)	2144 (-16)
5	EC 60 flat, 150 Watt, 48 v	EC 45 flat, 90 watt, 48 v	3	6	80	43.8 (10)	2315 (-9)
6	EC 60 flat, 150 Watt, 48 v	EC 45 flat, 80 watt, 60 v	4	6	80	40.97 (3)	2347 (-8)

tend to consume more energy. The first solution in Table II, for example is 24 percent lighter than the last, most energy-efficient solution in the table; however, it consumes 35 percent more energy.

C. Scenario C

In scenario B, we learned that reducing the gear ratios in the sun and ring branch by adding a stage to the differential can result in a more energy-efficient DMA. In scenario C, the sun and ring gearboxes can be eliminated entirely by increasing the gear ratio of the differential further, e.g. by adding more stages to the differential. Matex offers selected gearboxes with a maximum ratio of seven, so in order to develop a gearbox with a ratio of 50 or greater, at least three stages of these gear sets are required. A commercial gearbox with high efficiency and ratio makes more sense in this case. The Apex AB series gearboxes are two-stage planetary gearboxes with ratios of 50 up to 100, and efficiency of 94 percent and mass of 1.5 kilograms. These gearboxes have been considered as the output gearbox. In order to maximize the possible combinations of motors and gearboxes, the planetary gear set ratio is set to 3, 4, 5 and 7 for the available Matex planetary gear sets. The choice of spur gears with a ratio of 3 to 6 allows for a better combination of motors on the ring gear. The the gear ratio was limited to six to not obtain an excessively high diameter of the gears, and consequently in the differential. The possible combinations resulting from the simulation are depicted in Fig. 7. Table III describes the details of a number of combinations selected from the Pareto frontier.

The last row of Table III is 8 percent lighter than the first solution, and it consumes only 3 percent more energy. This combination is also lighter than the most lightweight solution in the scenario B at Table II, but it consumes significantly less energy. Compared to the scenario A at Table I, this solution is considerably lighter.

D. Discussion

The results clearly show that a trade-off exists between mass and energy efficiency. However, other factors need to be considered as well, such as whether or not the actuator will be mounted on a moving platform, and whether the obtained solutions have a reasonable volume and cost.

Also, as a design guideline, it can be observed from the results that IDX series motors were chosen in Tables I and II as an energy-efficient solution, despite their high weight. Additionally, flat series motors are preferred for lightweight solutions despite their rotor inertia being higher than IDX series motors with similar power density. Another recommendation for DMA design is to have no gearbox in between the motors and the differential, which may reduce the overall weight of the actuator.

In order to improve the methodology for selecting components of a dual-motor actuation system, there are several factors to consider. The calculated energy is the result of simulation over the mentioned torque-speed profile in Fig. 2. So the chosen trajectory will affect the actuator design. In other words, it means what percentage of the trajectory is in the high-torque region at low speed, what percentage is in the high-speed and low-torque region, and what percentage is the average torque-speed requirement. So, a smart way of choosing the trajectory is necessary for the design of an actuator that is more efficient. Also the optimal power distribution between two motors can be achieved by moving forward along the output trajectory step by step. However, this method does not guarantee a global optimal power distribution and it is computational time consuming, so it would be more appropriate to modify the method for optimal power distribution of two motors. Using Intel i7 processors (11th generation @3.00 GHz), the simulation took 13 hours and 40 minutes for Scenario A and about the same for Scenario B, but was reduced to 3 hours and 17 minutes for Scenario C which evaluated fewer combinations. Simulation time is affected by the overall trajectory duration, the sampling time interval, as well as the speed interval and its limit defined for the calculation of the optimal power distribution. Therefore, in future work, we will focus on developing a more computationally efficient methodology which does not rely on a search algorithm based on the trajectory.

E. Battery Mass

There is a trade-off between energy consumption and mass. This trade-off can, to some extent, be resolved if the robot is battery-powered, which is the case for e.g. mobile or wearable robots. In this situation, a higher energy consumption would need to be compensated by a heavier battery pack. Therefore, in this subsection, we will evaluate the total mass of the actuation system for different duration of the task, taking also battery mass into account.

Different battery technologies have different performance characteristics, and battery energy density plays a crucial role in determining the system's longevity. The energy density is determined by comparing its mass to the amount of energy it contains. Typically, this measurement is expressed in watt-hours

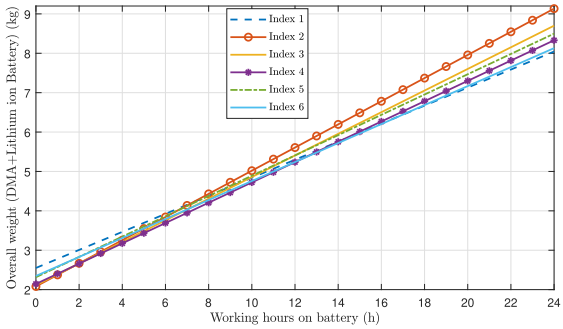

Fig. 8. Overall mass of 6 different combinations selected in Fig. 7 considering battery mass for up to 24 hours operation mode.

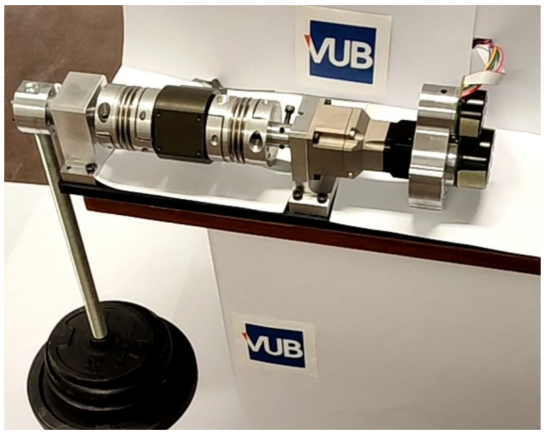

Fig. 9. Real-world implementation of the dual-motor actuator.

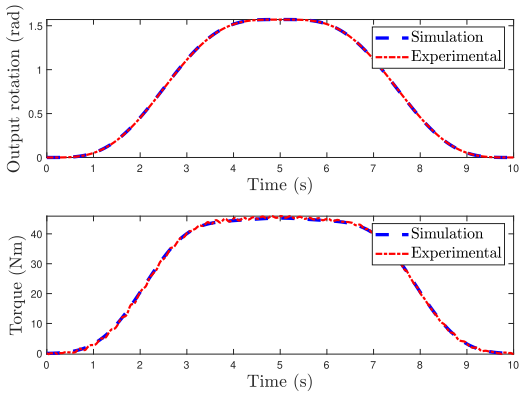

Fig. 10. The DMA performance in position and torque tracking of desired trajectory.

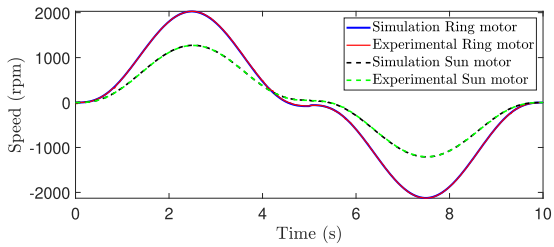

Fig. 11. The DMA performance in speed tracking of desired trajectory.

per kilogram (Wh/kg). The energy density of lithium-ion batteries, which are often selected for battery-powered robots, is approximately 170 Wh/kg on average [18]. This is the number that will be used in the calculations.

We calculated the energy consumption of the six selected combinations outlined in Table III and shown in Fig. 7. Battery mass is added to the mass of the combination, resulting in the overall mass of the combinations shown in Fig. 8. As expected, a lightweight actuator will result in the lightest overall solution for short-term use, while a more energy-efficient solution will have a lower overall mass for extended use. Around seven hours of operation represents the crossing point, so selecting the lightest actuator (second in Table III) or the most energy efficient (first in Table III) makes little difference. Also, the results indicate that the Index 6, as the final choice for long-term operation, behaves in a similar way to the global optimal energy solution (Index 1), despite utilizing a smaller motor for the ring gear. Hence, in this combination, we have the potential to design a more compact DMA.

V. Experimental Setup

An experimental setup was developed for the mentioned robot joint actuator. Fig. 9 illustrates the DMA coupled to a rod with a payload attached to it, which serves as the load. The DMA architecture corresponds to the one analyzed in this study. The planetary differential is composed of a Matex planetary gearset with ratio of 5 and a set of Nylatron (heat stabilized nylon) spur gears attached to the ring gear. The sun gear is driven by a Maxon EC60 flat 150-watt motor, while the ring gear is driven by a Maxon EC45 flat 80-watt motor. The ring drive-train is coupled to the ring using a 6:1 spur gear transmission. The output gearbox is an Apex AB series with ratio of 80. The actuator is coupled to a DRBK-100 torque sensor manufactured by ETH Messtechnik. A US Digital disk encoder (2000 CPT) measures the output rotation of the DMA.

A seventh-order polynomial trajectory was imposed, in which the output was varied from zero to 90 degrees of rotation in Fig. 10. According to the approach presented in section III, the energy-optimal trajectory of the sun and ring motors was extracted and applied as an input to the two motors using the inbuilt speed control mode of the Maxon EPOS4 controllers.

The measured torque on the torque sensor matches the simulation in Fig. 10, and the DMA precisely tracks the desired speed as depicted in Fig. 11. A comparison of the simulation and recorded electrical power of two motors illustrates the importance of the model in Fig. 12, as explained in detail in [10]. The simulation was conducted with some simplifications, e.g. assuming a constant efficiency value of the gearboxes, while in Fig. 12 you can see differences in negative power that illustrate the importance of considering a better model for components. Also, in positive power at high speeds, the power consumption of the sun motor differs from its simulated value. By analyzing these data, identifying different losses and improving the dynamic models of each component, we expect to build a more accurate model of the DMA in the future.

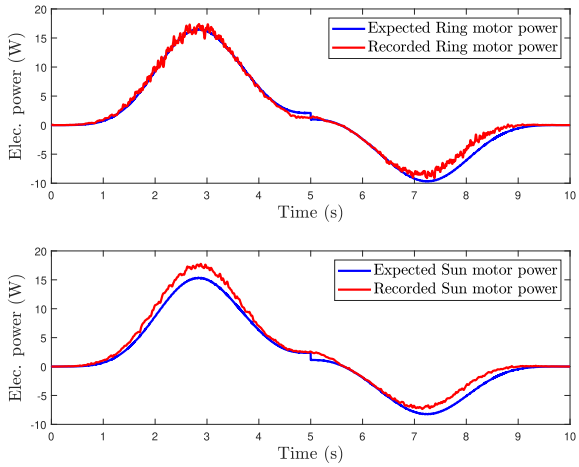

Fig. 12. Sun and ring motor electrical power as compared to what was predicted by simulation.

VI. Conclusion and Future Work

In this work, we have presented a methodology for designing dual-motor actuators. The methodology finds lightweight and energy-efficient combinations using all available input components. Three design scenarios were examined. A design with a high-ratio gearbox at the output of the differential and without gearboxes in the sun and ring drivetrain appeared to result in the most lightweight and energy-efficient solution.

Our results showed that mass and energy efficiency of the DMA were negatively correlated. To resolve the trade-off between mass and energy efficiency, we proposed to take the battery pack into account in the analysis. The analysis showed that, for long operating times, a heavier but more energy-efficient DMA will result in a robot with a lower total mass, whereas a lighter DMA is preferable for shorter operating times. In our use case, the crossing point was found to be at around 7 hours of operation.

While it is possible to select an actuator based solely on load and speed requirements and match random motors and gearboxes with them, the result will likely be heavy and inefficient. In simulations, it can be seen that many combinations are far from the Pareto frontier line. The design guidelines provided in this work are a first step to guiding designers towards the Pareto optimal solutions. These guidelines will be developed further in future work, as more mature prototypes will provide a more accurate view on the true mass of the DMA.

Experiments on a prototype indicate that the actuator model does not match entirely with the reality, as can be expected. Updating the dynamic model and investigating the impact of an improved model on the optimization procedure will be the subject of future work. In particular, we believe that a more accurate model of the transmissions, in particular the differential, could have a significant impact on the methodology. Additionally, the simulation trajectory should be chosen intelligently to cover all the robot's working points. A modification for determining the global optimal power distribution among two motors also helps to find more energy-efficient solutions.

References

[1] T. Verstraten, R. Furnémont, P. Lopez-Garcia, D. Rodriguez-Cianca, B. Vanderborght, and D. Lefeber, "Kinematically redundant actuators, a solution for conflicting torque–speed requirements," *Int. J. Robot. Res.*, vol. 38, no. 5, pp. 612–629, 2019.

[2] T. Verstraten et al., "Modeling and design of an energy-efficient dual-motor actuation unit with a planetary differential and holding brakes," *Mechatron.*, vol. 49, pp. 134–148, 2018.

[3] H. van de Straete, P. Degezelle, J. De Schutter, and R. Belmans, "Servo motor selection criterion for mechatronic applications," *IEEE/ASME Trans. Mechatronics*, vol. 3, no. 1, pp. 43–50, Mar. 1998.

[4] F. Roos, H. Johansson, and J. Wikander, "Optimal selection of motor and gearhead in mechatronic applications," *Mechatron.*, vol. 16, no. 1, pp. 63–72, 2006.

[5] S. Rezazadeh and J. W. Hurst, "On the optimal selection of motors and transmissions for electromechanical and robotic systems," in *Proc. IEEE/RSJ Int. Conf. Intell. Robots Syst.*, 2014, pp. 4605–4611.

[6] H. Giberti, S. Cinquemani, and G. Legnani, "Effects of the mechanical characteristics of the transmission on the choice of motor-reducers," *Mechatron.*, vol. 20, no. 5, pp. 604–610, Aug. 2010.

[7] H. Giberti, A. Clerici, and S. Cinquemani, "Specific accelerating factor: One more tool in motor sizing projects," *Mechatron.*, vol. 24, no. 7, pp. 898–905, 2014.

[8] A. Anderson, C. Richburg, J. Czerniecki, and P. Aubin, "A model-based method for minimizing reflected motor inertia in off-board actuation systems: Applications in exoskeleton design," in *Proc. IEEE 16th Int. Conf. Rehabil. Robot.*, 2019, pp. 360–367.

[9] G. Cusimano, "A procedure for a suitable selection of laws of motion and electric drive systems under inertial loads," *Mechanism Mach. Theory*, vol. 38, no. 6, pp. 519–533, 2003.

[10] T. Verstraten, R. Furnémont, G. Mathijssen, B. Vanderborght, and D. Lefeber, "Energy consumption of geared DC motors in dynamic applications: Comparing modeling approaches," *IEEE Robot. Automat. Lett.*, vol. 1, no. 1, pp. 524–530, Jan. 2016.

[11] T. Verstraten, G. Mathijssen, R. Furnemont, B. Vanderborght, and D. Lefeber, "Modeling and design of geared DC motors for energy efficiency: Comparison between theory and experiments," *Mechatron.*, vol. 30, pp. 198–213, 2015.

[12] F. Meoni and M. Carricato, "Optimal selection of the motor-reducer unit in servo-controlled machinery: A continuous approach," *Mechatron.*, vol. 56, pp. 132–145, 2018.

[13] G. Mathijssen et al., "SPEA introduction: Drastic actuator energy requirement reduction by symbiosis of parallel motors, springs and locking mechanisms," in *Proc. IEEE Int. Conf. Robot. Automat.*, 2016, pp. 676–681.

[14] A. Girard and H. H. Asada, "A two-speed actuator for robotics with fast seamless gear shifting," in *Proc. IEEE/RSJ Int. Conf. Intell. Robots Syst.*, 2015, pp. 4704–4711.

[15] V. Babin, C. Gosselin, and J.-F. Allan, "A dual-motor robot joint mechanism with epicyclic gear train," in *Proc. IEEE/RSJ Int. Conf. Intell. Robots Syst.*, 2014, pp. 472–477.

[16] K. Michaelis, B.-R. Höhn, and M. Hinterstoißer, "Influence factors on gearbox power loss," *Ind. Lubrication Tribol.*, vol. 63, no. 1, pp. 46–55, 2011.

[17] G. Enguerran, M. Abadi, and O. Alata, "An hybrid method for feature selection based on multiobjective optimization and mutual information," *J. Informat. Math. Sci.*, vol. 7, no. 1, pp. 21–48, 2015.

[18] Q. Abbas, M. Mirzaeian, M. R. Hunt, P. Hall, and R. Raza, "Current state and future prospects for electrochemical energy storage and conversion systems," *Energies*, vol. 13, no. 21, 2020, Art. no. 5847.